Chem. Senses 29: 411–424, 2004 DOI: 10.1093/chemse/bjh042

Characterization of Electro-olfactogram Oscillations and Their Computational Reconstruction

Noriyo Suzuki[1], Masakazu Takahata[1], Takayuki Shoji[2] and Yuko Suzuki[3]

[1]Animal Behavior and Intelligence, Division of Biological Sciences, Graduate School of Science, Hokkaido University, Sapporo 060-0810, Japan, [2]Department of Fisheries, School of Marine Science and Technology, Tokai University, Shimizu 424-8610, Japan and [3]Department of Oral Anatomy, School of Dentistry, Health Sciences University of Hokkaido, Ishikari-Tobetsu 061-0293, Japan

Correspondence to be sent to: Noriyo Suzuki, Animal Behavior and Intelligence, Division of Biological Sciences, Graduate School of Science, Hokkaido University, Sapporo 060–0810, Japan. e-mail: suzuki@sci.hokudai.ac.jp

Abstract

Electro-olfactogram (EOG) oscillations induced by odorant stimulation have been often reported in various vertebrates from fishes to mammals. However, the mechanism of generation of EOG oscillations remains unclear. In the present study, we first characterized the properties of EOG oscillations induced by amino acid odorants in the rainbow trout and then performed a computer simulation based on the main assumption that olfactory receptor neurons (ORNs) have intrinsic oscillatory properties due to two types of voltage-gated ion channels, which have not yet been reported in vertebrate ORNs. EOG oscillations appeared mostly on the peak and decay phases of negative EOG responses, when odorant stimuli at high intensity flowed regularly anterior to posterior olfactory lamellae in the olfactory organ. The appearance of EOG oscillations was dependent on the odorant intensity but not on the flow rate. The maximum amplitude and the maximum power frequency of EOG oscillations were 3.51 ± 3.35 mV (mean ± SD, n = 232, range 0.12–16.79 mV) and 10.59 ± 5.05 Hz (mean ± SD, n = 232, range 3.51–40.03 Hz), respectively. The simulation represented sufficiently well the characteristics of EOG oscillations; occurrence at high odorant concentration, odorant concentration-dependent amplitude and the maximum power frequency range actually observed. Our results suggest that EOG oscillations are due to the intrinsic oscillatory properties of individual ORNs, which have two novel types of voltage-gated ion channels (resonant and amplifying channels). The simulation program for Macintosh ('oscillation 3.2.4' for MacOS 8.6 or later) is available on the world wide web (http://bio2.sci.hokudai.ac.jp/bio/chinou1/noriyo_home.html).

Key words: computer simulation, EOG, olfactory receptor neuron, oscillation, subthreshold oscillation, voltage-gated ion channel

Introduction

Slow negative DC-voltage changes recorded from the surface of olfactory mucosa in response to odorants are termed electro-olfactograms (EOGs; Ottoson, 1958) and are regarded as compound receptor potentials of olfactory receptor neurons (ORNs) in the olfactory epithelium. Since the pioneering work on olfactory physiology by Adrian (1950), it has been observed that oscillations are often superimposed on EOGs (EOG oscillations) when odorants are applied at high concentrations: fishes (Tucker and Suzuki, 1972), amphibians (Ottoson, 1956, 1959; Takagi and Shibuya, 1960a,b, 1961; Hamilton and Kauer, 1989; Dorries and Kauer, 2000; Nakazawa *et al.*, 2000), reptiles (Tucker, 1975a,b; Lam *et al.*, 2000), birds (Shibuya and Tucker, 1967) and mammals (Adrian, 1955, 1956). The amplitude of EOG oscillations ranges from several hundreds microvolts to several millivolts and the dominant frequency varies from 10 to 60 Hz. In addition, EOG oscillations in the salamander are blocked by application of 1–10 μM tetrodotoxin (TTX) to the olfactory epithelium in a dose-dependent and reversible manner (Dorries and Kauer, 2000). Since EOG oscillations are observed both in *in vivo* olfactory mucosa preparations even after sectioning primary olfactory nerves and *in vitro* isolated olfactory mucosa preparations, they are apparently caused by populational activity of ORNs in the olfactory epithelium (Ottoson, 1958).

As to the generation mechanism of EOG oscillations, Ottoson (1956) first suggested that EOG oscillations might represent the oscillatory state of excitability within groups of ORNs of similar functional properties, since ORNs are densely packed in one layer, and consequently there are favorable conditions for interaction between active elements. However, Ottoson (1956) further implied that the appearance of EOG oscillations is the sign of a deteriorating preparation, because EOG oscillations do not appear until several hours after dissection or appear in preparations that are exhausted or damaged. Tucker (1975a,b) later examined the effects of anesthesia and oxygenation on the appearance of EOG oscillations in *in vivo* preparations and showed that they appear in rather robust preparations and their appearance is influenced by the depth of anesthesia and that there is a threshold of EOG amplitude for their appearance. Lettvin and Gesteland (1965) observed that the impulse activities of ORNs are suppressed by the application of negative current to the surface of olfactory mucosa that resulted in a potential shift of several millivolts negative, which is within the order of EOG amplitudes. A similar electrical stimulation experiment performed later by Juge *et al.* (1979) in the frog confirmed this observation. Together with the observation by Lettvin and Gesteland (1965), Tucker (1975a,b) postulated that EOG oscillations are initiated by EOG voltage stimulating electrically those ORNs that are not primarily involved in the generation of the EOG. A hypothesis different from that of Tucker (1975a,b) for the generation of the peripheral waves (PWs), i.e. the oscillatory activities of summated impulse responses from a small population of ORNs, was proposed recently by Parker *et al.* (1999): the oscillation is initiated by odorant-activated ORNs that drive loop currents through neighboring ORNs, thereby increasing the response thresholds of neighboring ORNs. Once adaptation of the initially activated ORNs takes place, the direction of the current inverts during stimulus presentation, because those ORNs that were previously inhibited by the loop current are now activated.

On the other hand, independent and intrinsic oscillatory activities due to the oscillatory properties of intracellular transduction cascade with a frequency range between 0.083 and 2.70 Hz have been observed in the voltage and current responses of isolated ORNs from the frog (Frings and Lindemann, 1988; Reisert and Matthews, 1997, 2001a), the mouse (Reisert and Matthews, 2001b) and the rainbow trout (Sato and Suzuki, 2000, 2001; Suzuki *et al.*, 2002). However, the frequency range of the oscillations in these studies is much lower than those of previously observed EOG oscillations and, therefore, the underlying mechanism of EOG oscillations might be different.

The characteristic frequency range of neural oscillations in different nervous systems is basically determined by two types of features: one is patterns of connectivity between neurons and the dynamic properties of the intervening synapses and the other is the network rhythmicity that arises via the coupling of oscillatory subunits, each of which possesses an intrinsically determined frequency preference. These two features are not mutually exclusive since the network connectivity could reinforce the patterns of excitation produced by coupled oscillators. The intrinsic frequency preference of a neuron is determined by its passive membrane properties and two different types of voltage-gated ion channels; resonant and amplifying channels, such as the slow-activated non-inactivating K^+ channel (e.g. outwardly rectifying K^+ channel) and the fast-activated non-inactivating Na^+ channel (e.g. persistent Na^+ channel), respectively (Hutcheon and Yarom, 2000).

To clarify the mechanism responsible for the generation of EOG oscillations, we first examined the characteristics of EOG oscillations induced by odorant stimulation with a quaternary mixture of amino acids in the rainbow trout to determine the odorant stimulation conditions that induce the EOG oscillations. We then performed a computer simulation based on the assumptions that the EOG is a local field potential composed of the summation of the time-lagged and exponentially weighed oscillatory receptor potentials of ORN groups. The ORNs were assumed to have intrinsic oscillatory properties due to their passive membrane properties and two types of voltage-gated ion channels that are activated by subthreshold depolarization of ORNs induced by the front-tail of odorant stimulation.

Materials and methods

EOG recordings from rainbow trout olfactory organs

Rainbow trout (*Onchorynchus mykiss*; fork length, 24–28 cm; weight, 100–270 g) obtained from a local fishery were lightly immobilized with i.m. injection of gallamine triethiodide (0.05–0.1 mg/100g body wt) and were fixed with a head clamp and rubber sponge cushion in an experimental box. The olfactory rosette of the left olfactory organ was exposed by removing the tissues covering the olfactory organ. The gill was constantly perfused with cooled and aerated tap water (12–15°C, DO 9.8 mg/l, 92.6% – 8.6 mg/l, 85.2%, DO9709; Delta OHM, Marconi) at a flow rate of 100 ml/min during the experiment. A plastic pipette electrode with a tip diameter of 300–500 μm, which was filled with 1% agarose gel–normal Ringer's solution (in mM: 100 NaCl, 3 KCl, 2 $CaCl_2$, 1 $MgCl_2$, 10 D-glucose, 5 HEPES and 2.2 NaOH, pH 7.4) and connected to a calomel bridge, was placed on the center of the olfactory rosette raphe to serve as an EOG recording electrode. Another plastic pipette electrode connected to a calomel bridge of similar dimension was placed on the head and served as a reference electrode. A silver–silver chloride (Ag–AgCl) plate was attached to the flank as a ground electrode. The olfactory rosette was continuously perfused with artificial well water (AWW; in mM: 0.5 NaCl, 0.05 KCl, 0.4 $CaCl_2$, 0.2 $NaHCO_3$, pH 6.9) (Shoji *et al.*, 2000) and stimulated by switching to odorant solutions with fixed durations; 1, 2, 3, 4, 5, 10 and 30 s, using

a self-made liquid odorant stimulator equipped with a PIC (peripheral interface controller) solenoid valve controller (Suzuki, 2002), to which Mariotte bottles of odorant solution reservoirs were connected with silicone tubings. Logarithmically diluted series of a quaternary mixture of amino acids (10 mM for each: L-Glu, L-Arg, L-Ala and L-Nva) in AWW were used as odorant stimuli. The stimulator outlet pipette, with an inner diameter of 200 μm, was positioned on the posterior edge of olfactory cavity, so as to allow the stimulus to flow evenly over a whole rosette in an posterior-to-anterior direction. Inspection of the stimulus flow with a dye solution (0.1% trypan blue) confirmed that the stimulus first flowed on the posterior floor of the olfactory cavity, flowed forward, bumped into the anterior edge and then turned backwards to the posterior edge of the olfactory cavity. The stimulus overflowed the lateral edge of olfactory cavity. The calibration of the waveforms of odorant pulses, by measuring liquid junction voltages with normal Ringer's solution in the dead fish killed with i.m. injection of an overdose of gallamine triethiodide, confirmed that the stimulus pulse actually had exponentially decaying front- and end-tails due to dilution by adapting AWW, which occurred during the flow through the tubing (see Simulation section). The duration of stimulus pulse was actually longer than that of the solenoid valve opening. The flow rate of adapting AWW and odorant stimuli was changed gravitationally by changing the vertical position between Mariotte reservoir bottle and the stimulator outlet pipette. Usually the position of the stimulator outlet pipette was fixed, while the position of the Mariotte reservoir bottles for adapting and stimulus solutions was changed by replacing them on different shelves at different heights. The flow rate in the experiment was thus changed stepwise from 3.4 to 6.0, 8.0, 10.0 and 12.6 ml/min. Another calibration by measuring the time difference between the appearance of junction potentials recorded in two different positions in the olfactory organ, using 0.1 M KCl or normal Ringer's solution, indicated that the flow rates 3.4, 8.0 and 12.6 ml/min corresponded roughly to the flow speeds 2.2, 7.3 and 12.5 mm/s, respectively. For the parameter values in the simulation section, the stimulation time-lags between seven ORN groups in the olfactory organ were estimated as 280, 180, 100, 80 and 70 ms for 3.4, 6.0, 8.0, 10.0 and 12.6 ml/min, respectively, where the length of the anteroposterior axis of the olfactory rosette is assumed to be ~5 mm. The range of the stimulus flow speed in the present study was likely even lower than that in natural condition because the average swimming speed of the rainbow trout with a 20–30 cm body length is ~70 cm/s and the inflow speed of water current from the anterior nares with a small diameter to the olfactory lamellae is presumably much higher (Bainbridge, 1960).

EOG signals were amplified by a conventional microelectrode amplifier (DC – 10 KHz) and acquired by PowerLab (ML-840, 4/20) through a digital low-pass filter (50 Hz) at 200 Hz sampling speed using Chart 3.6.9 (AD Instruments, Mountain View, CA).

Analysis of properties of EOG oscillations

The acquired signals were further processed through a digital high-pass filter (2 Hz) to isolate EOG oscillation signals. EOG oscillation data for a period of 5 s for Chart 3.6.9 were converted to the file format for Igor Pro 4.0.2 (WaveMetrics, Lake Oswego, OR), by which the oscillation data were further converted to the text file format for MEM 1.10 (Ishikawa, 2000) for continuous wavelet analyses using the 8th order Gabor (Gabor, 1946) and the Morlet (Morlet *et al.*, 1993) functions. The power density of the frequency for each record was analyzed at four levels, each of which was divided into 12 divisions, in the frequency range between 2.1 and 32.0 Hz for the 8th order Gabor function and 5.5 and 100.0 Hz for the Morlet function. The analyzed data for each record were displayed as an 8-bit gray scale diagram with frequency in Hz on the ordinate and time in seconds on the abscissa on a computer screen. The oscillation data in the waveforms produced by the simulation program (see below) were also subjected to continuous wavelet analyses as described above. The statistical evaluation of the amplitude and frequency of EOG oscillations was performed using StatView 4.5 (SAS Institute, Cary, NC).

Development of the simulation program

The simulation program of EOG responses for a Power Macintosh computer was developed with REALbasic 3.5J (REAL Software, Austin, TX) based on the following assumptions. (i) The EOG is a local field potential and is the summation of the time-lagged and exponentially weighted receptor potentials of ORN subpopulations in different loci on the horizontal plane of the olfactory epithelium. The subpopulations are arranged in a line along the moving direction of odorant stimulus flow. The olfactory epithelium in the rainbow trout is actually not a simple two-dimensional plane and there are normally seven rows of side-by-side arrangement of 14 olfactory lamellae along the anteroposterior axis of olfactory rosette (Yamamoto, 1982). Therefore, the number of ORN subpopulations is replaced by the number of rows of olfactory lamellae. Each row of ORN subpopulation is estimated to contain 70 000–140 000 individual ORNs of both types, ciliated and microvillous ORNs (Thommesen, 1983). (ii) The amplitude of receptor potentials of ORN subpopulations in different loci decays exponentially depending on the distance from the point of recording site. (iii) The odorant stimulus front-tail induces subthreshold oscillatory responses of ORN subpopulations prior to the arrival of the odorant stimulus body. The oscillatory frequency of an ORN subpopulation is determined by intrinsic oscillatory frequency preference for individual ORNs in the subpopulation. Here the depolarizing current to give the subthreshold oscillatory response of an ORN

subpopulation to the odorant stimulus front-tail is replaced by the current caused by EOG responses induced by the odorant stimulus body. Although the waveform for the subthreshold oscillation of individual ORNs in the ORN subpopulation is not shown in the following figures, the program described below can display the oscillation in detail by choosing an appropriate option.

In the simulation, we assumed further that the odorant flow stimulated all ORNs in a ORN group simultaneously, considering the velocity of odorant flow and the anatomical arrangement of olfactory lamellae in the olfactory rosette. The activity of each ORN subpopulation was considered to be the sum of synchronized receptor potential generated by all individual ORNs in the subpopulation. The simulated EOG was thus the sum of receptor potentials in seven ORN subpopulations that were activated successively as the odorant flowed over the olfactory epithelium.

The simulation program 'oscillation 3.2.4' (http://bio2.sci.hokudai.ac.jp/bio/chinou1/noriyo_home.html) is composed of four parts for producing the final simulation result. Every part of the program has corresponding screens on which different values for parameters and initial values can be set for numerical calculation. The calculations in different parts are combined in the program to produce the final simulation result. Briefly, the first part of the program is displayed on the 'Set parameters' screen, which is essentially the same as the previously developed program cAMP 9.2.8 (Suzuki *et al.*, 2002), where the parameters for the stimulus intensity and the time course of EOG waveform as a whole can be set. The second part is the 'Set population parameters' screen, where the parameters for the number of ORN subpopulations, the exponentially decaying factor for EOG responses in different loci, the attenuation factor for addition of the subthreshold oscillation and the stimulation time-lag between the ORN groups, which depends on the stimulus flow speed, can be set. The third is the 'Set subthreshold parameters' screen, where the parameters for the passive properties of the ORN, the activation properties of the fast-activated non-inactivating Na^+ channel and the slow-activated non-inactivating K^+ channel and the time-scale factor for fine adjustment of the frequency of the subthreshold oscillation, can be set. Most of the default parameter values in the 'Set subthreshold parameters' screen are for a typical cortical neuron in mammals (Gutfreund *et al.*, 1995). The last is the 'Simulation result' screen, on which the conversion ratio of the sum of the concentrations of activated CNG-channel and Ca^{2+}-activated Cl^--channel (Suzuki *et al.*, 2002) to the electrical current to induce the subthreshold oscillation of the ORN subpopulations and the stimulus duration can be set (see the Appendix for the algorithm for calculations in the program). On the 'Simulation result' screen, the summation of time-lagged and exponentially weighed EOG responses is expressed as the relative and dimensionless value on ordinate versus the time in sec on abscissa. With the 'show subthreshold responses' button turned on by clicking it to change to 'hide subthreshold responses', the subthreshold responses of individual ORNs will be displayed on the screen together with the EOG as the summation of each ORN subpopulation response. The frequency of subthreshold oscillation of individual ORNs was almost the same as those of oscillations of both ORN subpopulation and EOG. The polarity and scale of the ordinate for the simulation result are changeable to represent the actual EOG responses. The time scale of the abscissa is also changeable up to 100 s. The simulation result data can be exported as text files for Chart 3.6.9 at different sampling rates, usually 200 Hz.

The oscillation data of simulated EOG responses produced by oscillation 3.2.4 were further processed by Igor Pro 4.0 and subjected to continuous wavelet analyses by MEM 1.10. The numerical solutions for the differential equations in the program were calculated with the Euler integration method (Gershenfeld, 1999; de Schutter, 2001) on a fixed integration time step, usually 0.1 ms or shorter, using parameters set on the four different screens. We used some of the parameter values in the references cited in the review articles (Zufall *et al.*, 1994; Nakamura, 2000) for the 'Set parameters' screen and in other references (Schild and Restrepo, 1998; Madrid *et al.*, 2003; Pun and Kleene, 2003) for the 'Set subthreshold parameters' screen, although we used mostly empirically determined parameter values after many trials and errors during the program execution.

All graphs obtained by different software packages in the present study were further processed for presentation using Canvas 6 graphics software (Deneba, Miami, FL).

Results

Recording condition of stimulus-driven EOG oscillations

EOG oscillations driven by odorant stimulation were observed in ~50% (25/51) of rainbow trout lightly immobilized with gallamine triethiodide. Oscillations usually appeared just after finishing the preparation set-up and continued to appear during the period when the robust blood circulation in the capillaries of olfactory lamellae was clearly visible under a microscope. Oscillations mostly disappeared in the later period of the experiment when the amplitude of EOG responses to the odorant stimuli at the same intensity became smaller than at the early part of the recording. The blood circulation in the capillaries of olfactory lamellae decreased to become only faintly visible, which was interpreted as a sign of deterioration of the preparation. Inspection of the odorant stimulus flow visualized by adding trypan blue dye into the stimulus solution during the period of appearance of oscillations confirmed that the stimulus flowed regularly along the anteroposterior axis of the olfactory rosette, similar to the odorant stimulus flow through anterior to posterior nares in the natural fish environment.

Characteristics and amplitude of EOG oscillations

Oscillations appeared when the odorant stimuli at high concentration in the range between $10^{-3.0}$ and $10^{-2.0}$ M were applied at various flow rates. A total of 232 oscillation records from 25 fish were analyzed for their amplitude and frequency. The maximum amplitude of oscillations increased with increased stimulus intensity (P = 0.073, Mann–Whitney U-test, $10^{-3.0}$ M, n = 3 versus $10^{-2.0}$ M, n = 16), as the amplitude of EOG responses increased with increased stimulus intensity. The duration of oscillations also increased to some extent with increased stimulus concentration (Figure 1A,B). The maximum amplitude of oscillations correlated with the amplitude of EOG responses ($P < 0.001$, Spearman's correlation = 0.863; Pearson's correlation = 0.763, n = 232). However, the maximum amplitude of oscillations and the amplitude of EOG responses were dependent on the stimulus intensity, but not on the stimulus flow rate (Figure 2). Their amplitudes were 3.15 ± 3.35 mV (n = 232, range = 0.12–16.79 mV) and 21.39 ± 12.56 mV (n = 232, range = 0.86–48.90 mV) in the range between $10^{-3.0}$ and $10^{-2.0}$ M, respectively. Once an oscillation appeared in a preparation, it continued to appear for 3–4 h (for 7 h in one case), in response to odorant stimulus pulses (Figure 3). Oscillations mostly appeared on the peak of EOG responses and decayed with the decay of EOG responses (on the peak, 59.5%, n = 138; after the peak, 30.2%, n = 70; before the peak, 10.3%, n = 24). The phasic response characteristic of oscillations was also noted when the stimulus duration was longer than 10 s (Figure 4).

Frequency of EOG oscillations

The wavelet analyses of oscillations showed that oscillations had a basic frequency band with a high power density and often a second harmonics band with a lower power density (Figs 1C for $10^{-2.0}$ M and 2C). Since the power density of the basic frequency bands was much higher than that of the second harmonics bands, the former bands of oscillations were mainly analyzed in this study. The temporal position of the maximum power frequency of oscillations, i.e. the central frequency of the basic frequency bands with a maximum power density, varied from one record to the other but mostly localized on the peak of EOG responses.

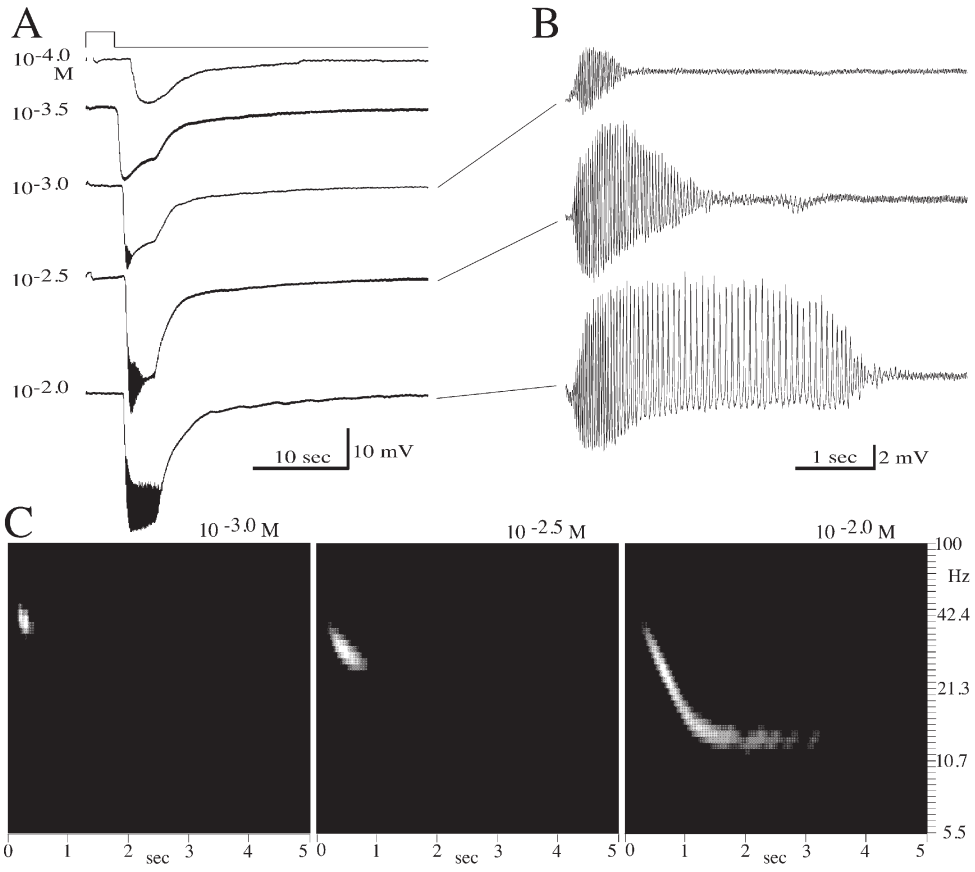

Figure 1 EOG responses to the quaternary amino acid mixture at different intensities. **(A)** EOG responses to the amino acid mixture at various stimulus intensities ($10^{-4.0}$–$10^{-2.0}$ M; duration = 3 s; flow rate = 8.0 ml/min). Stimulus intensity (M) is shown on each trace. Top trace shows the timing of stimulus pulse. **(B)** The corresponding oscillations to the records in A were processed by filtering through a digital high-pass-filter (2 Hz). The maximum amplitude of oscillations increased with increased stimulus intensity. **(C)** The power density diagrams in 8-bit gray scale analyzed by the Morlet function. The diagrams were obtained from the records in B. Maximum power frequency for the diagrams: 40.0, 30.1 and 21.3 Hz for $10^{-3.0}$, $10^{-2.5}$ and $10^{-2.0}$ M, respectively. Note the second harmonics band with a lower power density in the oscillation for $10^{-2.0}$ M stimulus.

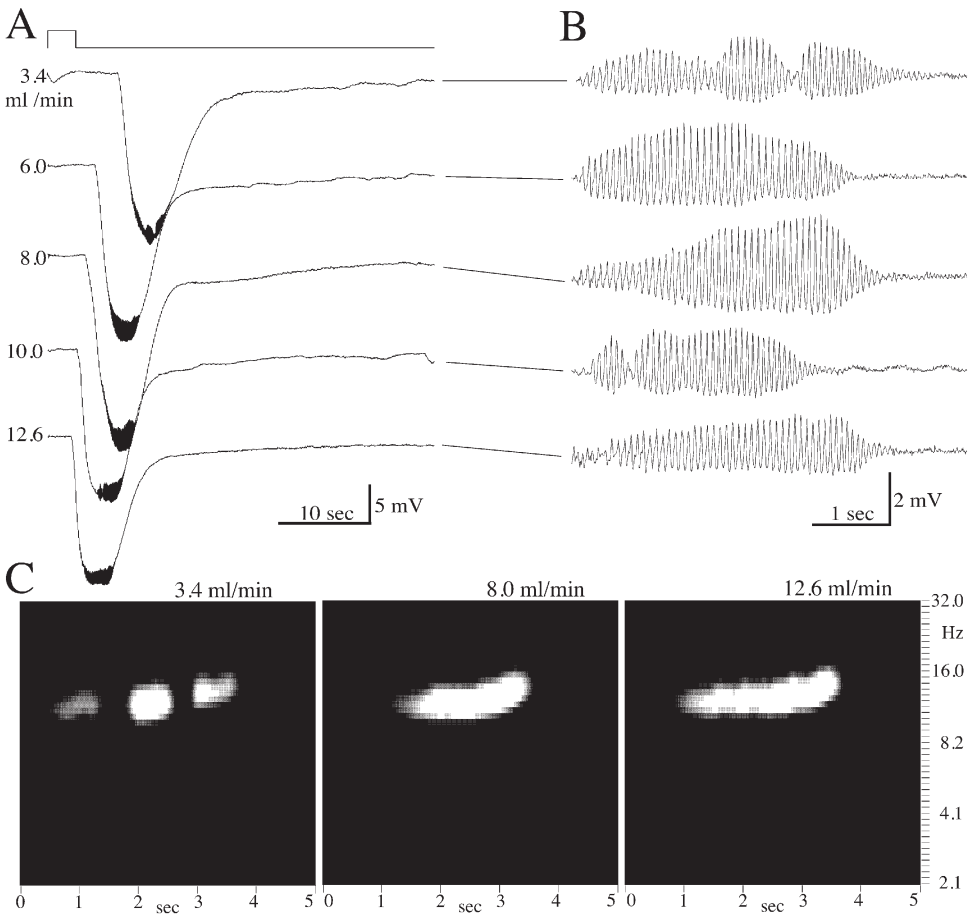

Figure 2 EOG responses to the quaternary amino acid mixture at different stimulus flow rates. **(A)** EOG responses at different stimulus flow rates. Stimulus flow rate was changed from 3.4 to 12.6 ml/min (intensity = $10^{-2.0}$ M; duration = 3 s). Stimulus flow rate (ml/min) is shown on each trace. Top trace shows the timing of stimulus pulse. **(B)** The corresponding oscillations to the records in A were processed by filtering through a digital high-pass filter (2 Hz). The maximum amplitude and the maximum power frequency of oscillations did not change significantly. **(C)** The power density diagrams in 8-bit gray scale analyzed by the 8th order Gabor function. The diagrams were obtained from the records in B. The maximum power frequencies for the diagrams are 11.52, 12.89 and 12.89 Hz for 3.4, 8.0 and 12.6 ml/min, respectively. Note the second harmonics bands with a low power density in the oscillations.

The basic frequency band of oscillations also tended to move down with time during the oscillation period and showed a higher frequency in the initial phase of oscillations (Figure 1C). The lower and upper limits of the basic frequency bands were 6.21 ± 3.44 Hz (n = 232, range = 2.14–26.75 Hz) and 29.06 ± 8.70 Hz (n = 232, range = 16.01–67.18 Hz) in the intensity range between $10^{-3.0}$ and $10^{-2.0}$ M, respectively. The maximum power frequency of oscillations was 10.59 ± 5.06 Hz (n = 232, range = 3.51–40.03 Hz) in the intensity range between $10^{-3.0}$ and $10^{-2.0}$ M. Although the upper limit of the basic frequency bands did not change significantly with increased stimulus intensity, the lower limit of the basic frequency bands significantly decreased with increased stimulus intensity (P = 0.007, $10^{-3.0}$ M, n = 3 versus $10^{-2.0}$ M, n = 16; P = 0.005, $10^{-2.5}$ M, n = 10 versus $10^{-2.0}$ M, n = 16, Mann–Whitney U-test). The maximum power frequency of the oscillations tended to lower with increased stimulus intensity (P = 0.033, $10^{-3.0}$ M, n = 3 versus $10^{-2.0}$ M, n = 16; P = 0.020, $10^{-2.5}$ M, n = 10 versus $10^{-2.0}$ M, n = 16, Mann–Whitney U-test; Figure 1C). However, there were no significant differences in the upper and the lower limits of the basic frequency bands and in the maximum power frequency of oscillations, when the odorant stimuli were applied at different flow rates of 3.4–12.6 ml/min (Figure 2).

Simulation of EOG oscillations

As described in Materials and methods, the simulation program oscillation 3.2.4 was developed based on several assumptions. The program was composed of four calculation parts with the corresponding parameter setting screens: 'Set parameters', 'Set population parameters', 'Set subthreshold parameters' and 'Simulation result'. After many trials and errors during the program execution, the following parameter values other than default parameter values for the different parameter setting screens were empirically determined to represent the characteristics of actual EOG oscillations. On the 'Set parameters' screen, *os* (rate of odorant binding to receptor), os_2 (rate of odorant dissociation from receptor) and *A3max* (maximal *a3* at saturating calcium ion concentration) (Suzuki *et al.*, 2002) were

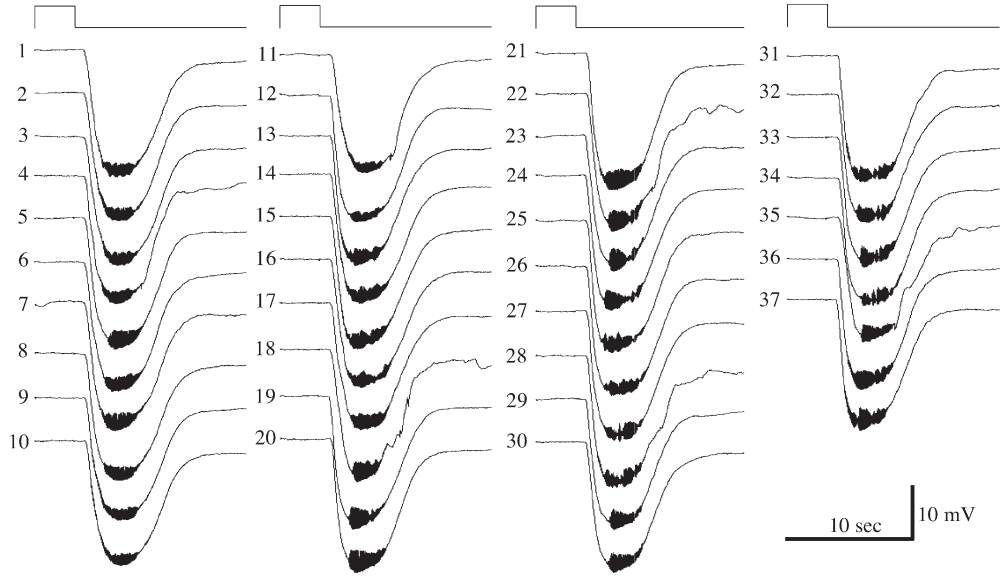

Figure 3 Consecutive records of EOG oscillations. Olfactory rosette was stimulated repetitively with the quaternary amino acid mixture at $10^{-2.0}$ M intensity (duration = 3 s, flow rate = 8.0 ml/min) at an interval of 2 min. Number on each record indicates the number of order of stimulation. Top trace on each column shows the timing of stimulus pulse.

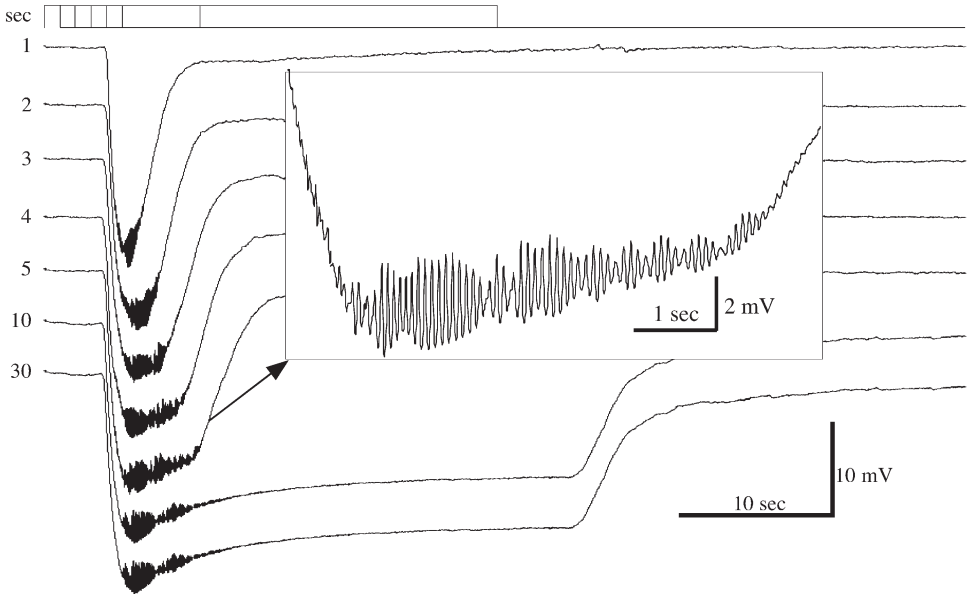

Figure 4 EOG responses to the quaternary amino acid mixture at different stimulus durations. Stimulus duration was changed stepwise from 1 to 30 s (intensity = $10^{-2.0}$ M, flow rate = 8.0 ml/min). Number on each record represents the stimulus duration in seconds. Top traces on the records indicate timing of stimulus pulses. Inset shows the magnified figure of the record of 5 s stimulation for clear visualization of the oscillation. The oscillation decays with the decay of EOG response, indicating that the oscillations are phasic, especially for stimulus duration >10 s.

set at 0.003 μM/s, 0.7/s and 0.1/s, respectively, to represent the characteristic time course of actual EOG responses. On the 'Set population parameters' screen, the number of subpopulations, interval from stimulus onset time (stimulation time-lag between ORN subpopulations), which depends on the stimulus flow rate or speed, and the attenuation factor for addition, were set at 7, 100 ms for 8.0 ml/min and 0.007, respectively. On the 'Set subthreshold parameters' screen, C (membrane capacitance), g_L (leak conductance), G_{Na} (maximal Na^+ conductance), G_K (maximal K^+ conductance) and s (time scaling parameter) were set at 0.01 nF, 0.0005 μS, 0.001 μS, 0.013 μS and 0.0107, respectively. The values for C and g_L were similar to those for ORNs estimated in the references (Schild and Restrepo, 1998; Madrid *et al.*, 2003; Pun and Kleene, 2003) but the values for G_{Na}, G_K and s were as small as 1/20, 1/6 and 1/20 compared to those used for simulation for a typical cortical neuron of mammals (Gutfreund *et al.*, 1995). On the 'Simulation

result' screen, the concentration (μM) to current (nA) ratio was set at 0.132. Figure 5A illustrates the simulated EOG oscillations with an average maximum power frequency in actual EOG oscillations recorded in the present study. The amplitude of simulated EOG responses increased with increased stimulus intensity and the oscillations appeared in the intensity range $>10^{-3.0}$ M. The maximum amplitude of the oscillations increased with increased stimulus intensity and the duration of the oscillations also increased slightly with increased stimulus intensity (Figure 5B). The maximum power frequency of the oscillations was ~10 Hz. The second harmonics bands with a lower power density at ~20 Hz were also observed (Figure 5C). These characteristics of the simulated EOG oscillations were essentially similar to those of actual EOG responses to amino acid odorant stimuli at high intensity (Figure 1), although there was no obvious decrease of the maximum power frequency with increased stimulus intensity.

For the simulation of EOG oscillations to odorant stimuli at different flow rates, *s* (time scaling parameter) on the 'Set subthreshold' screen was changed to 0.013, but the other parameters were left unchanged at the above-mentioned values. The interval from stimulus onset time (stimulation time-lag between ORN groups) on the 'Set population parameters' screen was varied stepwise from 280 to 180, 100, 80, and 70 ms, which corresponded roughly to the actual flow rates of 3.4, 6.0, 8.0, 10.0 and 12.6 ml/min, respectively. Figure 6A illustrates the simulated EOG oscillations to odorant stimuli at different stimulation time-lag between ORN subpopulations, where odorant stimulus intensity and duration were kept constant at $10^{-2.0}$ M and 3 s, respectively. The amplitude of simulated EOG responses did not change with changes of stimulation time-lag. Figure 6B shows that the maximum amplitude of oscillations did not change significantly over the range of stimulation time-lag, although the oscillations were slightly jaggy unlike actual EOG oscillations. The maximal power frequency of oscilla-

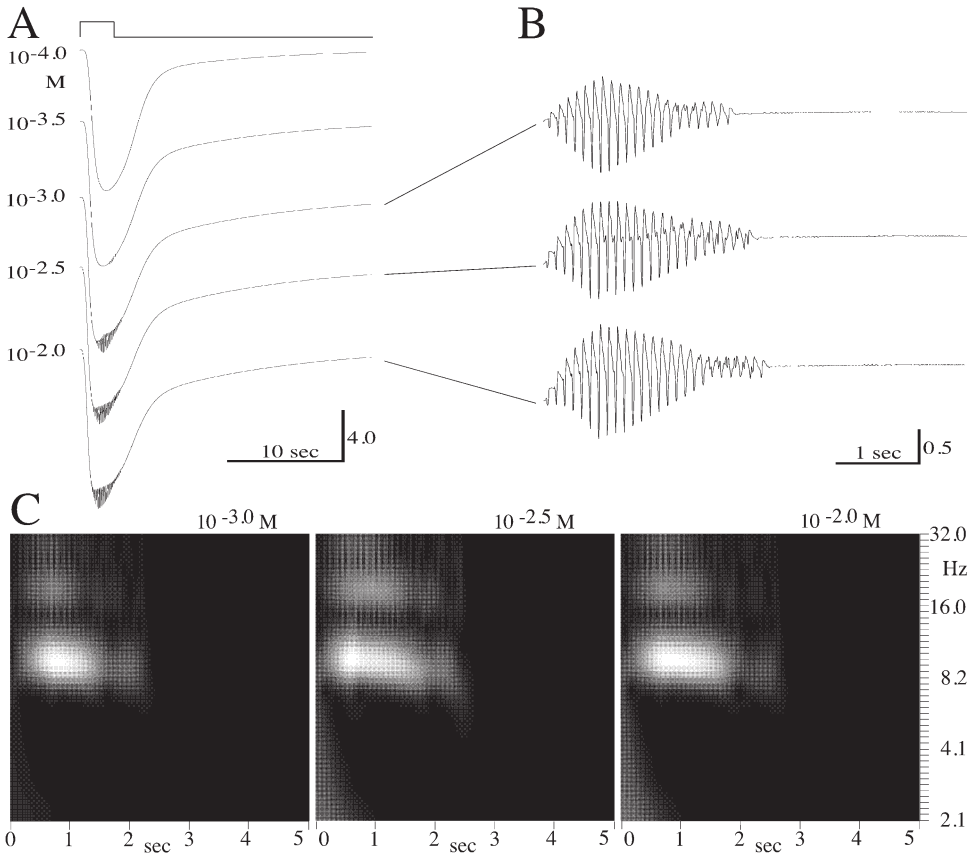

Figure 5 Simulated EOG oscillations to odorants at high stimulus intensity when the parameters for number of ORN groups and stimulation time-lag were set at 7 and 100 ms, respectively (see text for setting of other parameters). **(A)** EOG responses to odorants in the intensity range between $10^{-4.0}$ and $10^{-2.0}$ M. The oscillations appeared in the intensity range $>10^{-3.0}$ M. Top trace shows stimulus timing pulse of 3 s duration. Stimulus intensity (*M*) is shown on each trace. Numbers on vertical calibration bars in A and B denote the relative value. **(B)** The corresponding oscillations to the traces in A were processed by filtering through a digital high-pass filter (2 Hz). The maximum amplitude of simulated oscillations increased with increased stimulus intensity. **(C)** Power density diagrams in 8-bit gray scale analyzed by the 8th order Gabor function. The diagrams were obtained from the traces in B. The maximum power frequencies for the diagrams are 9.57, 9.57 and 10.15 Hz for $10^{-3.0}$, $10^{-2.5}$ and $10^{-2.0}$ M, respectively. Note the second harmonics bands with a lower power density in the oscillations.

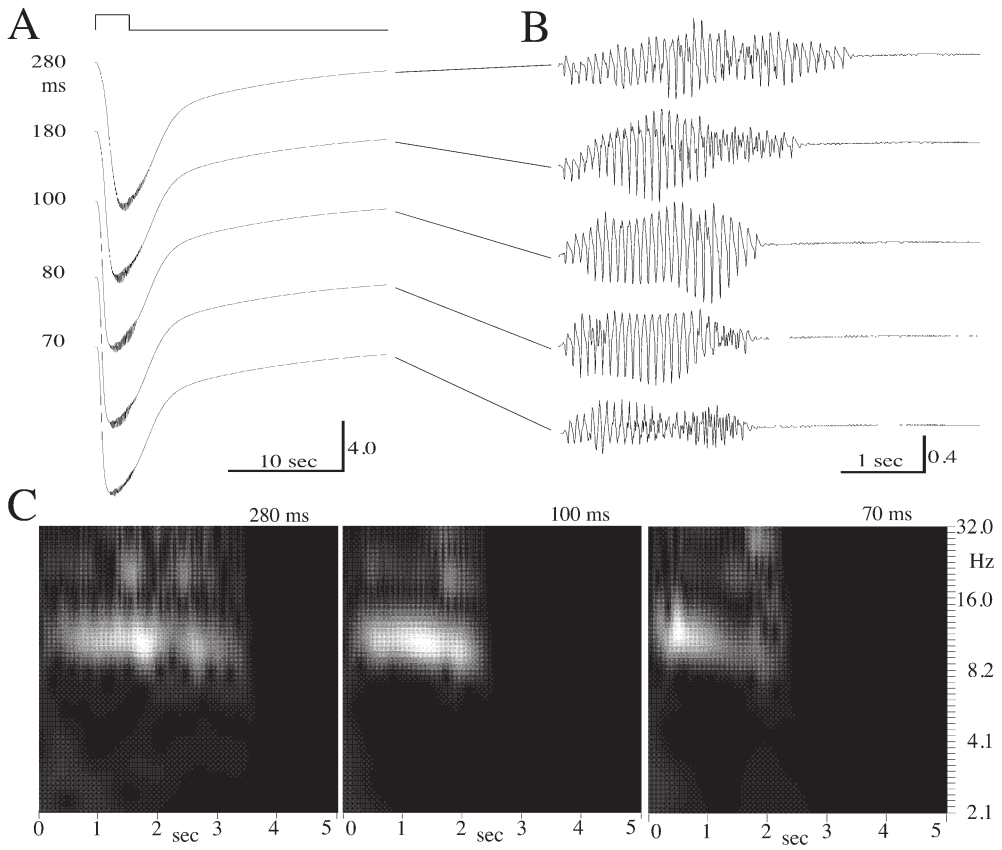

Figure 6 Simulated EOG oscillations to odorants at different stimulation time lags (intensity = $10^{-2.0}$ M; duration = 3 s; see text for setting of other parameters). **(A)** EOG responses to odorants at different stimulation time-lags, 280, 180, 100, 80 and 70 ms, which correspond roughly to flow rates of 3.4, 6.0, 8.0, 10.0 and 12.6 ml/min, respectively. The amplitude of simulated EOG responses did not change significantly over the range of stimulation time-lag. Top trace shows stimulus timing pulse. Numbers on vertical calibration bars in A and B denote the relative value. **(B)** The corresponding oscillations to the traces in A were processed by filtering through a digital high-pass filter (2 Hz). The maximum amplitude of simulated oscillations did not change significantly over the range of stimulation time-lag. **(C)** The power density diagrams in 8-bit gray scale analyzed by the 8th order Gabor function. The diagrams obtained from the traces for 280, 100 and 70 ms in B are shown. The maximum power frequencies for the diagrams are 10.74, 10.74 and 11.52 Hz for 280, 100 and 70 ms, respectively. Note the second harmonics bands with a lower power density in the oscillations.

tions also did not change significantly over the range of stimulation time-lag, and the second harmonics bands with a lower power density were also observed (Figure 6C). These characteristics of simulated EOG oscillations to odorant stimuli at different stimulation time-lags corresponded roughly with those of actual EOG responses to odorant stimuli at different flow rates (Figure 4A–C).

For the simulation of EOG oscillations with the frequency range actually observed in the present study, the combinations of parameter values of s (time scaling parameter) on the 'Set subthreshold parameters' screen and concentration (μM)/current (nA) ratio on the 'Simulation result' screen were selected for 0.007 and 0.14, 0.013 and 0.132, and 0.065 and 0.20, respectively, while values for other parameters were kept as above. Figure 7A–C shows such simulation results for EOG oscillations with different maximum power frequencies. The resulting maximum power frequencies were 3.71, 10.74 and 40.03 Hz, respectively. Each frequency value corresponded to that of the lowest, average and highest maximum power frequency actually observed in the present study.

Discussion

EOG oscillations are not signs of deterioration

In the present study, EOG oscillations were recorded from ~50% of physiologically active fish lightly immobilized with gallamine triethiodite. The fish appeared to be well oxygenated, as judged by the blood circulation in capillaries of olfactory lamellae. The odorant stimulus flowed regularly along the anteroposterior axis of the olfactory rosette. Since the amplitude of the EOG was as large as ~20 mV in response to the $10^{-3.0}$–$10^{-2.0}$ M quaternary amino acid mixture, the responsiveness of ORNs to odorants might be quite high. EOG oscillations to odorants in the toad occur only during the period of breeding migration season, when the responsiveness of ORNs to odorants might be enhanced by hormonal control (Nakazawa *et al.*, 2000). Such increased responsiveness of ORNs to odorants was not the

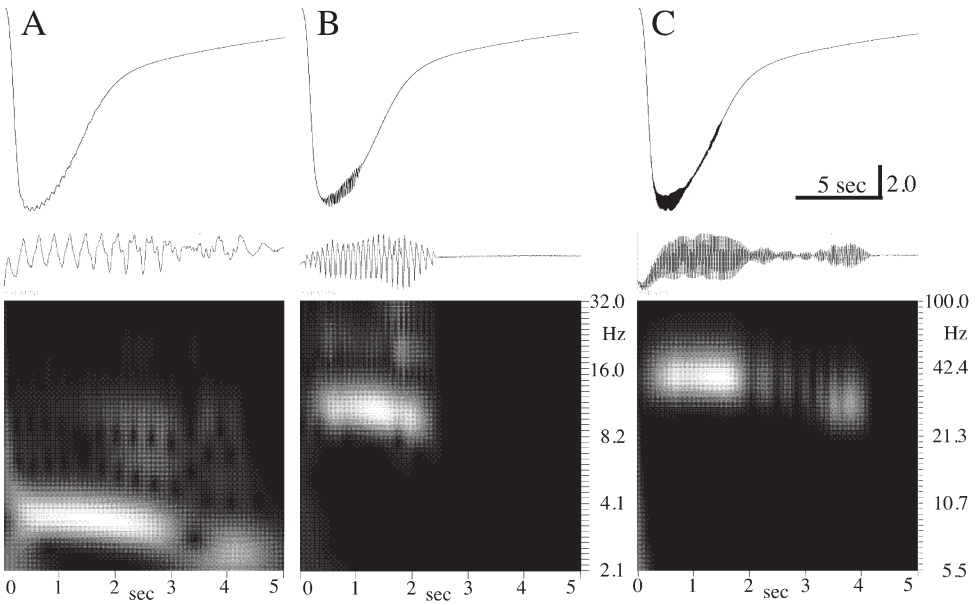

Figure 7 Simulated EOG oscillations with different maximum power frequencies (intensity = $10^{-2.0}$ M; duration = 3 s). The parameters for number of ORN groups and stimulation time-lag were set at 7 and 100 ms, respectively (see text for the setting of other parameters). **(A–C)** Simulated EOG oscillations and their power density diagrams in 8-bit gray scale analyzed by the 8th order Gabor (A and B) and the Morlet function (C). The maximum power frequencies for A, B and C are 3.71, 10.74 and 40.03 Hz, respectively.

case in the immatured rainbow trout in the present study, but the high responsiveness of ORNs to odorants might be at least necessary for the appearance of EOG oscillations. Thus, in contrast to the impression by Ottoson (1956), the appearance of EOG oscillations, as indicated by Tucker (1975a,b), is not a sign of a deteriorating preparation. The success rate for recording EOG oscillations in the present study (~50%), however, was lower than in the previous study on the salamander (~94%, 34/36; Dorries and Kauer, 2000). The success rate for recording EOG oscillations in the present study was also lower than that for recording peripheral waves (PWs) in the catfish (~83%, 38/46; Nikonov *et al.*, 2002), which have similar lamellar structure of olfactory epithelium as do the rainbow trout (Yamamoto, 1982; Thommesen, 1983). Thus, the reason for large difference in success rate for recording oscillations between different vertebrates was unclear at the moment.

Comparison with previously observed EOG oscillations

The maximum amplitude of EOG oscillations in rainbow trout recorded in the present study (3.51 ± 3.35 mV, mean ± SD, n = 232, range = 0.12–16.79 mV) was within the order of the amplitude of EOG oscillations observed in different vertebrates, although the types of odorant stimuli used in previous studies, either gaseous or liquid, were different (Adrian, 1955, 1956; Ottoson, 1956, 1959; Takagi and Shibuya, 1960a,b, 1961; Shibuya and Tucker, 1967; Tucker and Suzuki, 1972; Tucker, 1975a,b; Hamilton and Kauer, 1989; Dorries and Kauer, 2000; Lam *et al.*, 2000; Nakazawa *et al.*, 2000). The maximum power frequency of EOG oscillations in the rainbow trout in the present study (10.59 ± 5.05 Hz, mean ± SD, n = 232, range = 3.51–40.03 Hz) was also comparable to those of catfish (~30 Hz; Tucker and Suzuki, 1972), frogs and toads (10–25 Hz; Ottoson, 1956, 1959; Takagi and Shibuya, 1960a,b, 1961; Nakazawa *et al.*, 2000), salamanders (12–17 Hz; Hamilton and Kauer, 1989; Dorries and Kauer, 2000) and tortoise and turtles (10–14 Hz; Tucker, 1975a,b; Lam *et al.*, 2000). However, the maximum power frequency in the present study was slightly lower than those of birds (~36 Hz; Shibuya and Tucker, 1967) and rabbits (40–60 Hz; Adrian, 1955, 1956). Thus, the frequency of EOG oscillations is likely to be higher in homoiotherms than in poikilotherms. In addition, the maximum power frequency of EOG oscillations (~10 Hz) in the rainbow trout that live in cold waters was slightly lower than that of the PWs of the catfish that live in warm waters (28.5 Hz; Nikonov *et al.*, 2002). Therefore, it is suggested that such differences are due to differences in temperature-dependent mechanisms underlying EOG oscillations, such as temperature-dependence of ion channel activity involved in the oscillatory frequency preference of ORNs.

Mechanism of generation of EOG oscillations

The simulation in the present study represented sufficiently well the characteristics of true EOG oscillations, including the phasic nature of the oscillations. The main assumption for the simulation was that individual ORNs in the olfactory epithelium have intrinsic oscillatory properties based on their passive membrane properties and resonant and amplifying ion channel activities, by which their frequency preference is determined (Hutcheon and Yarom, 2000). The resonant and amplifying ion channels of ORNs were

assumed to be activated by the odorant stimulus front-tail coming prior to the stimulus body. The stimulus front-tail induces the subthreshold depolarization of neighboring ORNs not yet stimulated by the following stimulus body. The oscillation caused by the stimulus front-tail was the essential assumption in the present simulation. This assumption that the subthreshold depolarization occurs in neighboring ORNs was in contrast to the previous hypotheses by Tucker (1975a,b) and Parker *et al.* (1999) with respect to the initial current direction. They assumed that EOG oscillations and PWs are initiated by the suppression of ORNs by the hyperpolarizing current caused by odorant-activated ORNs. Once the ORNs that are first activated become adapted, the direction of the current inverts during stimulus presentation, due to the activation of those ORNs that were previously suppressed by the hyperpolarizing current. Such bi-stable current pattern would have given a tonic oscillation during odorant presentation, although the oscillation could be phasic due to adaptation of ORNs. However, actual EOG oscillations recorded in the present study were phasic especially for longer stimulus duration than 10 s.

Parameter setting in the simulation

To represent well the characteristics of actual EOG oscillations, many of parameter values were empirically determined after many trials and errors during execution of the program, oscillation 3.2.4. The parameter settings on the 'Set subthreshold parameters' screen were most important to determine the frequency range of EOG oscillations, especially those values of C (membrane capacitance), g_L (leak conductance), G_{Na} (maximal Na^+ conductance), G_K (maximal K^+ conductance) and s (time scaling parameter). Although the values for C and g_L used here were similar to those estimated in recent electrophysiological studies on vertebrate ORNs (Madrid *et al.*, 2003; Pun and Kleene, 2003), the values for the other parameters (G_{Na}, G_K and s) were empirically determined as 0.001 μS, 0.013 μS and 0.007–0.065, respectively. These values for G_{Na}, G_K and s were as small as 1/20, 1/6 and ~1/30–1/3 compared with those used for simulation for a typical cortical neuron of mammals (Gutfreund *et al.*, 1995). Such small values for G_{Na} and G_K for the present simulation of EOG oscillations, conversely, may explain the reason why such voltage-gated ion channels have not yet been found in the membrane of vertebrate ORNs in the previous electrophysiological studies (Schild and Restrepo, 1998). In addition, Dorries and Kauer (2000) showed that EOG oscillations in the salamander were blocked by the application of 1.0–10 μM TTX to the olfactory epithelium in a dose-dependent and reversible manner, suggesting that TTX-sensitive voltage-gated Na^+ channels might be involved in EOG oscillations. Therefore, future electrophysiological studies are expected to confirm the distribution of such voltage-gated ion channels with small conductances for resonant and amplifying channels, such as slow-activated non-inactivating K^+ channel (e.g. outwardly rectifying K^+ channel) and fast-activated non-inactivating Na^+ channel (e.g. persistent Na^+ channel), in the membrane of vertebrate ORNs.

Behavioral and physiological significance of EOG oscillations

In the present study, EOG oscillations occurred when amino acid odorants at high concentrations flowed regularly from the anterior to posterior lamellae. The threshold for appearance of EOG oscillations was $10^{-3.0}$ M of quaternary amino acid mixture. This range of odorant intensity is within the range of saturation of the dose–response relations for integrated olfactory bulb responses to many single amino acids in the rainbow trout (Hara, 1982). In the catfish, the PWs, which have a similar frequency to those of simultaneously recorded local EOG oscillations, were also induced by single amino acids such as methionine and alanine at concentrations in the mM range. Addition of 0.1–1 mM trisodium citrate to the amino acid stimulus solution enhanced the appearance of PWs (Parker *et al.*, 2000). Tucker (1975b) claimed that EOG oscillations may be caused by physiologically excessive stimulation and thus in that sense represent an epiphenomenon. However, it is probable that amino acid odorants at mM concentrations are detected by fish as odorant cues for close localization of food source, although the cosummatory behaviors including biting and snapping followed by the appetitive behaviors such as searching and swimming in the center of chemical plume of amino acids are initiated by the activation of taste system but not by the activation of the olfactory system both in the rainbow trout and catfish (Valentincic and Caprio, 1997; Valentincic *et al.*, 2000). Thus, the concentration range in which EOG oscillations occur is apparently physiologically excessive as noted by Tucker (1975b), but may serve somehow as meaningful olfactory cues in the fish feeding behaviors. On the other hand, simultaneous recordings of EOG oscillations or PWs and summated impulse responses of small populations of neurons at different bulbar loci (local field potentials, LFPs) to volatile odorants in the salamander (Dorries and Kauer, 2000) and amino acid odorants in the catfish (Nikonov and Caprio, 2001; Nikonov *et al.*, 2002) have shown that the PWs and LFPs are cross-correlated; the frequency and magnitude of the LFPs increased with PWs and their oscillations are phase-locked. These studies suggest that the oscillations of both levels share a common source and are modulated together and that their common source might be the oscillatory properties of individual ORNs in the olfactory epithelium. Furthermore, the recent studies on the chemotopical map of the olfactory bulb as measured by EEGs, optical imaging or single neuron responses from the olfactory bulb to behaviorally relevant odorants in different salmonid fishes (Hara and Zhang, 1998), in the zebrafish (Friedrich and Korsching, 1998) and in the catfish (Nikonov and Caprio, 2001; Hansen *et al.*, 2003) have shown that different olfactory bulb regions respond preferentially to the

specific classes of odorants, such as amino acids, bile salts and nucleotides, prostaglandins and steroids; the odorant quality information for different classes of odorants are relayed to the different loci of the olfactory bulb by morphologically different types of ORNs (ciliated, microvillous and crypt) which might have different transduction cascades. In this respect, therefore, EOG oscillations induced by amino acid odorants in the present study should influence oscillatory activity in the specific region of olfactory bulb and thus might be involved in the odorant quality coding in fishes.

Appendix

The simulation result displayed on the 'Simulation result' screen of oscillation 3.2.4 is the final calculation result combining the calculations in four parts of the program. The simulation result (Y) is the summation of time-lagged and exponentially weighed EOG responses and is expressed as the relative and dimensionless value in the following equations.

$$Y = X + a \times Z \tag{1}$$

where

$$X = b \times r \tag{2}$$

when $N \leq N_0$ or

$$r = g_{\mathrm{Max}} \times \exp((N - N_0)/L)$$

when $N > N_0$

$$r = g_{\mathrm{Max}} \times \exp(-(N - N_0)/L)$$

The terms used above are defined in Table A1.The calculation algorithm for Z (replaced by V in the following) is as follows. An ORN is assumed to be represented by a single compartment consisting of a capacitor, a passive membrane conductance (g_{L}) and two time- and voltage-gated conductances, one for Na^+ (G_{Na}) and the other for K^+ (G_{K}). The Na^+ conductance, which is activated faster than the K^+ conductance, is assumed to be activated instantaneously, reducing the number of ordinary differential equations into two (White *et al.*, 1995):

$$\frac{\mathrm{d}V}{\mathrm{d}t} = (-1/C) \times (g_{\mathrm{L}} + G_{\mathrm{Na}} \times m_0) \times V + (G_{\mathrm{K}} \times E_{\mathrm{K}}/C) \times W - (G_{\mathrm{K}}/C) \times V \times W + (g_{\mathrm{L}} \times E_{\mathrm{L}} + G_{\mathrm{Na}} \times m_0 \times E_{\mathrm{Na}} - I_{\mathrm{app}})/C \tag{3}$$

$$\frac{\mathrm{d}W}{\mathrm{d}t} = s \times (w_0 - W)/T \tag{4}$$

Table A1 Definition of terms

Y	Summation of time-lagged and exponentially weighed EOG responses
X	Time-lagged and exponentially weighed EOG responses
a	Attenuation factor
Z	Subthreshold oscillations of ORN subpopulations
b	Sum of concentrations of activated CNG-channel and Ca^{2+}-activated Cl^--channel (cAMP 9.2.8; Suzuki *et al.*, 2002)
r	Weighing coefficient
g_{Max}	Maximal weight at N_0
N	Number of ORN subpopulations
N_0	Center number of ORN subpopulation
L	Length constant

Table A2 Definition of parameters, their dimensions and initial values for numerical calculation

Initial values		
V	Membrane potential [mV]	–65
W	Activation coefficient of G_{K}	0.001
Parameters		
C	Membrane capacitance [nF]	0.25
g_{L}	Leak conductance [μS]	0.025
G_{Na}	Maximal Na^+ conductance [μS]	0.022
G_{K}	Maximal K^+ conductance [μS]	0.084
s	Time scaling parameter	0.2
I_{app}	Applied current [nA]	
E_{L}	Reversal potential of leak conductance [mV]	–65
E_{Na}	Reversal potential of Na^+ conductance [mV]	+40
E_{K}	Reversal potential of K^+ conductance [mV]	–80
E_1	Half-activation voltage of Na^+ conductance [mV]	–40
E_2	Slope of Na^+ conductance activation function [mV]	5
E_3	Half-activation voltage of K^+ conductance [mV]	–35
E_4	Slope of K^+ conductance activation function [mV]	10
m_0	Steady state activation function of Na^+ conductance	
w_0	Steady state activation function of K^+ conductance	
T	Activation time constant of K^+ conductance [ms]	

where

$$m_0 = \left(1 + \frac{\exp((V-E_1)/E_2) - \exp((E_1-V)/E_2)}{\exp((V-E_1)/E_2) + \exp((E_1-V)/E_2)}\right)/2$$

$$w_0 = \left(1 + \frac{\exp((V-E_3)/E_4) - \exp((E_3-V)/E_4)}{\exp((V-E_3)/E_4) + \exp((E_3-V)/E_4)}\right)/2$$

$$T = \exp((V-E_3)/(2E_4)) + \exp((E_3-V)/(2E_4))$$

For actual numerical calculation in equation (3), I_{app} was replaced by $b \times c$, where c was introduced as the conversion ratio of sum of concentrations of activated CNG-channel and Ca^{2+}-activated Cl^--channel (μM) to the electrical current (nA) in oscillation 3.2.4. Definition of parameters, their dimensions and initial values for numerical calculation are shown in Table A2. Initial values and parameters in Table A2 were taken from Gutfreund *et al.* (1995) and most of them were set as default values on the 'Set subthreshold parameters' screen of oscillation 3.2.4.

Acknowledgements

We thank Dr Yasuhiro Ishikawa (Ishikawa Medical Clinic, Saitama, Japan) for his kind guidance during the use of MEM wavelet analysis software. We also thank Dr Toshio Kumazawa (Graduate School of Environmental Earth Science, Hokkaido University) for providing us a DO meter and Dr Shin Tochinai (Graduate School of Science, Hokkaido University) for the maintenance of our web site (http://bio2.sci.hokudai.ac.jp/bio/chinou1/).

References

Adrian, E.D. (1950) *The electrical activity of the mammalian olfactory bulb.* EEG Clin. Neurophysiol., 2, 377–388.

Adrian, E.D. (1955) *Potential oscillations in the olfactory organ*. J. Physiol. (Lond.), 128, 21P–22P.

Adrian, E.D. (1956) *The action of the mammalian olfactory organ.* J. Laryngol. Otol., 70, 1–14.

Bainbridge, R. (1960) *Speed and stamina in three fishes.* J. Exp. Biol., 37, 129–153.

de Schutter, E. (2001) Computational Neuroscience: Realistic Modeling for Experimentalists. CRC Press, Boca Raton, FL.

Dorries, K.M. and **Kauer, J.S.** (2000) *Relationships between odor-elicited oscillations in the salamander olfactory epithelium and olfactory bulb*. J. Neurophysiol., 83, 754–765.

Friedrich, R.W. and **Korsching, S.I.** (1998) *Chemotopic, combinatorial and noncombinatorial odorant representations in the olfactory bulb revealed using a voltage-sensitive axon tracer*. J. Neurosci., 18, 9977–9988.

Frings, S. and **Lindemann, B.** (1988) *Odorant response of isolated olfactory receptor cells is blocked by amiloride*. J. Membr. Biol., 105, 233–243.

Gabor, D. (1946) *Theory of communication.* J. IEE, 93, 429–457.

Gershenfeld, N. (1999) The Nature of Mathematical Modeling. Cambridge University Press, Cambridge.

Gutfreund, Y., Yarom, Y. and **Segev, I.** (1995) *Subthreshold oscillations and resonant frequency in guinea-pig cortical neurons: physiology and modelling*. J. Physiol. (Lond.), 483, 621–640.

Hamilton, K.A. and **Kauer, J.S.** (1989) *Patterns of intracellular potentials in salamander mitral/tufted cells in response to odor stimulation*. J. Neurophysiol., 62, 609–625.

Hansen, A., Rolen, S.H., Anderson, K., Morita, Y., Caprio, J. and **Finger, T.E.** (2003) *Correlation between olfactory receptor cell type and function in the channel catfish.* J. Neurosci., 23, 9328–9339.

Hara, T.J. (1982) *Structure-activity relationships of amino acids as olfactory stimuli.* In Hara, T.J. (ed.), Chemoreception in Fishes. Elsevier, Amsterdam, pp. 135–180.

Hara, T.J. and **Zhang, C.** (1998) *Topographic bulbar projections and dual neural pathways of the primary olfactory neurons in salmonid fishes*. Neuroscience, 82, 301–313.

Hutcheon, B. and **Yarom, Y.** (2000) *Resonance, oscillation and the intrinsic frequency preferences of neurons*. Trends Neurosci., 23, 216–222.

Ishikawa, Y. (2000) Wavelet Analysis for Clinical Medicine. Igaku-Shuppan, Tokyo [in Japanese].

Juge, A., Holley, A. and **Delaleu, J.C.** (1979) *Olfactory receptor cell activity under electrical polarization of the nasal mucosa in the frog. I. Spontaneous activity*. J. Physiol. (Paris), 75, 919–927.

Lam, Y.-W., Cohen, L.B., Wachowiak, M. and **Zochowski, M.R.** (2000) *Odors elicit three different oscillations in the turtle olfactory bulb.* J. Neurosci., 20, 749–762.

Lettvin, J.Y. and **Gesteland, R.C.** (1965) *Speculations on smell.* In Frisch, L. (ed.), Cold Spring Harbor Symposia on Quantitative Biology, Vol. 30, Sensory Receptors. Cold Spring Harbor Laboratory of Quantitative Biology, Cold Spring Harbor, L.I., New York, pp. 217–225.

Madrid, R. Sanhueza, M., Alvrez, O. and **Bacigalupo, J.** (2003) *Tonic and phasic receptor neurons in the vertebrate olfactory epithelium.* Biophys. J., 84, 4167–4181.

Morlet, D., Peyrin, F., Desseigne, P., Touboul, P. and **Rubel, P.** (1993) *Wavelet analysis of high-resolution signal-averaged ECGs in postinfarction patients.* J. Electrocardiol., 26, 311–320.

Nakamura, T. (2000) *Cellular and molecular constituents of olfactory sensation in vertebrates*. Comp. Biochem. Physiol. A, 126, 17–32.

Nakazawa, H., Kaji, S. and **Ishii, S.** (2000) *Oscillatory electric potential on the olfactory epithelium observed during the breeding migration period in the Japanese toad,* Bufo japonicus. Zool. Sci., 17, 293–300.

Nikonov, A.A. and **Caprio, J.** (2001) *Electrophysiological evidence for a chemotopy of biologically relevant odors in the olfactory bulb of the channel catfish*. J. Neurophysiol., 86, 1869–1876.

Nikonov, A.A., Parker, J.M. and **Caprio, J.** (2002) *Odorant-induced olfactory receptor neural oscillations and their modulation of olfactory bulbar responses in the channel catfish*. J. Neurosci., 22, 2352–2362.

Ottoson, D. (1956) *Analysis of the electrical activity of the olfactory epithelium*. Acta Physiol. Scand., 35(Suppl. 122), 1–83.

Ottoson, D. (1958) *The slow response of the olfactory end organs.* Exp. Cell Res., Suppl. 5, 451–459.

Ottoson, D. (1959) *Comparison of slow potentials evoked in the frog's nasal mucosa and olfactory bulb by natural stimulation*. Acta Physiol. Scand., 47, 149–159.

Parker, J.M., Lindemann, B. and **Caprio, J.** (1999) *Electrical communication among olfactory receptor neurons by peripheral waves [abstract]*. Chem. Senses, 24, 576.

Parker, J.M., Chang, Q. and **Caprio, J.** (2000) *Citrate enhances olfactory receptor responses and triggers oscillatory receptor activity in the channel catfish*. J. Neurophysiol., 83, 2676–2681.

Pun, R.Y.K. and **Kleene, S.J.** (2003) *Contribution of cyclic-nucleotide-gated channels to the resting conductance of olfactory receptor neurons*. Biophys. J., 84, 3425–3435.

Reisert, J. and **Matthews, H.R.** (1997) *Effects of sodium removal on the oscillatory response to prolonged stimulation in frog olfactory receptor cells*. J. Physiol. (Lond.), 499, 88P.

Reisert, J. and **Matthews, H.R.** (2001a) *Responses to prolonged odour stimulation in frog olfactory receptor cells*. J. Physiol. (Lond.), 534, 179–191.

Reisert, J. and **Matthews, H.R.** (2001b) *Response properties of isolated mouse olfactory receptor cells.* J. Physiol. (Lond.), 530, 113–122.

Sato, K. and **Suzuki, N.** (2000) *The contribution of a Ca^{2+}-activated Cl^- conductance to amino-acid-induced inward current responses of ciliated olfactory neurons of the rainbow trout*. J. Exp. Biol., 203, 253–262.

Sato, K. and **Suzuki, N.** (2001) *Whole-cell response characteristics of ciliated and microvillous olfactory receptor neurons to amino acids, pheromone candidates and urine in rainbow trout*. Chem. Senses, 26, 1145–1156.

Schild, D. and **Restrepo, D.** (1998) *Transduction mechanisms in vertebrate olfactory receptor cells*. Physiol. Rev., 78, 429–466.

Shibuya, T. and **Tucker, D.** (1967) *Single unit responses of olfactory receptors in vultures.* In Hayashi, T. (ed.), Olfaction and Taste II. Pergamon Press, New York, pp. 219–233.

Shoji, T., Ueda, H., Ohgami, T., Sakamoto, T., Katsuragi, Y., Yamauchi, K. and **Kurihara, K.** (2000) *Amino acids dissolved in stream water as possible home stream odorants for masu salmon.* Chem. Senses, 25, 533–540.

Suzuki, N. (2002) *PIC solenoid valve controller for olfactory and taste stimulation [in Japanese]*. Jpn. J. Taste Smell Res., 9, 195–199.

Suzuki, N., Takahata, M. and **Sato, K.** (2002) *Oscillatory current responses of olfactory receptor neurons to odorants and computer simulation based on a cyclic AMP transduction model*. Chem. Senses, 27, 789–801.

Takagi, S.F. and **Shibuya, T.** (1960a) *Potential oscillations in the lower olfactory pathway of the toad*. Nature (Lond.), 186, 724.

Takagi, S.F. and **Shibuya, T.** (1960b) *The potential oscillations observed in the olfactory epithelium, nerve and bulb to the toad and frog*. Jpn. J. Physiol., 10, 499–508.

Takagi, S.F. and **Shibuya, T.** (1961) *Studies on the potential oscillation appearing in the olfactory epithelium of the toad*. Jpn. J. Physiol., 11, 23–27.

Thommesen, G. (1983) *Morphology, distribution, and specificity of olfactory receptor cells in salmonid fishes*. Acta Physiol. Scand., 117, 241–249.

Tucker, D. (1975a) *Waves elicited from peripheral neural tissue (olfactory) in response to odorous stimulation [abstract]*. Biophys. J., 15, 271a.

Tucker, D. (1975b) *The role of respiratory ventilation in reliably obtaining electrical waves from olfactory mucosa and nerve in response to odorous stimulation*. In Ichioka, M. (ed.), Proceedings of the 9th Japanese Symposium on Olfaction and Taste, The Japanese Association for the Study of Taste and Smell (JASTS), Osaka (Tokyo), pp. 16–17.

Tucker, D. and **Suzuki, N.** (1972) *Olfactory responses to Schreck–Stoff of catfish*. In Schneider, D.(ed.), Olfaction and Taste IV. Wissenschaftliche Verlagsgesellschaft, Stuttgart, pp. 121–127.

Valentincic, T. and **Caprio, J.** (1997) *Visual and chemical release of feeding behavior in adult rainbow trout*. Chem. Senses, 22, 375–382.

Valentincic, T., Metelko, J., Ota, D., Pirc, V. and **Blejec, A.** (2000) *Olfactory discrimination of amino acids in brown bullhead catfish.* Chem. Senses, 25, 21–29.

White, J.A., Budde, T. and **Kay, A.R.** (1995) *A bifurcation analysis of neuronal subthreshold oscillations.* Biophys. J., 69, 1203–1217.

Yamamoto, M. (1982) *Comparative morphology of the peripheral olfactory organ in teleosts.* In Hara, T.J. (ed.), Chemoreception in Fishes. Elsevier, Amsterdam, pp.39–59.

Zufall, F., Firestein, S. and **Shepherd, G.M.** (1994) *Cyclic nucleotide-gated ion channels and sensory transduction in olfactory receptor neurons.* Annu. Rev. Biophys Biomol. Struct., 23, 577–607.

Accepted March 31, 2004